Title: ZO1 scaffold isoforms differentially contribute to electrical synapse formation

Authors: Jennifer Carlisle Michel, Margaret M. B. Grivette, Amber T. Harshfield, Lisa Huynh, Bradley Loomis, Kaitlan McKinnis, Brennen T. Miller, Tiffany W. Huang, Sophia Lauf, Mia E. Michel, Audrey J. Marsh, Lila E. Kaye, Rachel M. Lukowicz-Bedford, Dylan R. Farnsworth, E. Anne Martin, and Adam C. Miller*

* = corresponding author
Institute of Neuroscience, University of Oregon, United States

Abstract
Electrical synapses are neuronal gap junction channels associated with a macromolecular complex called the electrical synapse density (ESD), which regulates development and dynamically modifies electrical transmission. However, the molecular mechanisms of ESD formation are not well understood. Using the Mauthner cell of zebrafish as a model, we previously found that the intracellular scaffolding protein ZO1 is a member of the ESD, localizing postsynaptically, where it is required for channel localization, electrical communication, neural network function, and behavior (Lasseigne et al., 2021). Here, we show that the complexity of the ESD is further diversified by the genomic structure of the ZO1 gene locus. The ZO1 gene is alternatively initiated at three transcriptional start sites resulting in isoforms with unique N-termini that we call ZO1b-Alpha, -Beta, and -Gamma. We demonstrate that ZO1b-Beta is localized to electrical synapses where it is necessary and sufficient for robust channel localization. By contrast, ZO1b-Gamma is localized to synapses yet plays a minor role in electrical synapse formation. This study expands the notion of molecular complexity at the ESD, revealing that an individual genomic locus can contribute multiple independent isoforms that differentially contributing to electrical synaptogenesis. We propose that ESD complexity, at the level of the proteome, but also in the diversity of individual protein isoforms, will have critical impacts on the structure, function, and plasticity of electrical transmission.

Introduction
Fast synaptic communication in vertebrates is mediated by both electrical and chemical synapses (Moroz and Kohn, 2016; Pereda, 2014; Ryan and Grant, 2009). At electrical synapses, plaques of gap junction (GJ) channels mediate direct ionic communication between cells, while chemical synapses use neurotransmitter release and reception. The development and function of both synaptic types are supported by a dense network of associated proteins, called the electrical synapse density (ESD) and postsynaptic density (PSD), respectively (Ackermann et al., 2015; Grant, 2019; Lasseigne et al., 2021; Marsh et al., 2017; Martin et al., 2020; Miller et al., 2015; Siddiqui and Craig, 2011). Decades of research have identified hundreds of distinct proteins in the PSD, including the extensively studied family of membrane-associated guanylate kinases (MAGUKs, e.g., PSD-95, SAP102, etc), which dynamically regulate the structure and function of chemical synapses (González-Mariscal et al., 2000; Zheng et al., 2011; Zhu et al., 2016). Electron micrographs of neuronal tissue suggest an equally rich and

complex regulatory network complementing each side of electrical synapses (Brightman and Reese, 1969), though few ESD proteins have been identified to date. We recently showed that the ZO1 intracellular scaffold, a MAGUK, is an ESD protein that localizes postsynaptically at zebrafish electrical synapses, where it directly interacts with neuronal Connexins and is required for channel localization, electrical communication, neural network function, and behavior (Lasseigne et al., 2021). Here we show that ZO1 exists at electrical synapses in distinct isoforms, encoded by unique transcriptional start sites, unlocking an additional layer of ESD complexity. We show that one isoform is necessary and sufficient for channel localization, while the other, though present, has little impact on synapse formation. These results suggest that ESD scaffold complexity balances distinct actions of development and regulation, drawing parallels to PSD scaffold diversity at chemical synapses.

Results and Discussion

Alternatively initiated isoforms of the *tjp1b/ZO1b gene* are expressed in the Mauthner cell circuit

Our recent work demonstrated that the ZO1b scaffold is required postsynaptically for Connexin localization at zebrafish Mauthner cell electrical synapses (Lasseigne et al., 2021; Marsh et al., 2017). Located on chromosome 25, the *tjp1b/ZO1b* gene is a complex locus with three distinct initiation sites annotated on public databases (Ensembl) that predict three transcripts of varying lengths (Fig. 1A). Each transcript contains a unique first exon, which includes 5'UTR and start codon, and each has a varying number of additional exons incorporated before splicing into a common exon and the remaining transcript and 3'UTR (exons 5-31; Fig. 1B). While each transcript predicts a unique N-terminal protein translation, all three retain the assortment of common Membrane Associated Guanylate Kinase (MAGUK) protein-protein interaction modules including PDZs, SH3, GUK, and ZU5 domains (Fig. 1C). We wondered if *tjp1b/ZO1b* locus complexity contributed to electrical synapse proteomic diversity.

Alternatively initiated transcripts can indicate differences in tissue-specific or developmental expression. Inspection of the spatiotemporal expression pattern of *tjp1b/ZO1b* through early development using our single cell RNA-seq atlas (Farnsworth et al., 2020) revealed broad expression of the *tjp1b/ZO1b* transcript, suggesting broad usage of the gene in different tissues over time (Fig. S1A). The chemistry used for the atlas data (10X Genomics) is heavily biased toward the 3' end of genes preventing analysis of the alternatively initiated transcripts, so we turned to probes designed to detect the unique first exons of each isoform. Using fluorescent RNA *in situ* on wildtype 5 day post fertilization (dpf) whole fish, we observed robust expression of *tjp1b/ZO1b-Beta* and *tjp1b/ZO1b-Gamma* transcripts in the brain and spinal cord (Fig. S1B). We also see overlapping expression in other areas, such as skin, otolith, and jaw. From this data we conclude that *tjp1b/ZO1-Beta and tjp1b/ZO1b-Gamma* transcripts may be the main isoforms expressed in neuronal tissue.

We next addressed which *tjp1b/ZO1b* isoforms are expressed in neurons of the Mauthner circuit. This circuit drives a fast escape response to threatening stimuli and is

composed of two Mauthner cells in each animal that each receive multimodal sensory input that is then relayed to spinal cord circuitry to drive turns (Eaton et al., 1977; Jacoby and Kimmel, 1982; Liu and Fetcho, 1999). Mauthner makes prominent, stereotyped, electrical synapses with auditory afferents on its lateral dendrite (Club endings, CEs) (Bartelmez and Hoerr, 1933; Pereda et al., 2004; Yao et al., 2014) and also with Commissural Local (CoLo) interneurons of the spinal cord (M/CoLo) (Chie Satou et al., 2009). We looked for *tjp1b/ZO1b* isoform expression in the Mauthner and CoLo cell body of 5 dpf wildtype fish harboring the enhancer trap transgene *zf206Et (*Fig. 1D-K). Signals for *tjp1b/ZO1b-Beta* and *tjp1b/ZO1b-Gamma* transcripts were readily observed in both Mauthner and CoLo cell bodies (Fig. 1H-K). Signal for *tjp1b/ZO1b-Alpha* transcript was not detected in Mauthner or CoLo but instead in unidentified nearby cells in the neural tube (white arrow, Fig. 1F,G). We conclude that *tjp1b/ZO1b-Beta* and *tjp1b/ZO1b-Gamma* are expressed in Mauthner and CoLo, making them candidates for electrical synapse formation, while *tjp1b/ZO1b-Alpha* may play a role outside of the circuit.

ZO1b-Beta and ZO1b-Gamma localize to electrical synapses

To determine if unique transcripts led to distinct protein expression in the Mauthner cell circuit we used CRISPR to insert a V5 epitope tag at the N-terminus of each *tjp1b/ZO1b* isoform and looked for V5 staining in the Mauthner cell circuit of 5 dpf larvae. First, we found that using CRISPR/Cas9-induced homology directed repair with a short, single nucleotide repair oligo resulted in animals with frequent insertion of the V5 epitope tag into the locus of interest (Fig. S1C). These injections resulted in animals with mosaic V5 labeling of electrical synapses and cell membranes throughout the animal (Fig. S1D-G). Using this mosaic approach, we found that both V5-ZO1b-Beta and V5-ZO1b-Gamma were expressed in cells of the nervous system, and localized to Mauthner electrical synapses (Fig. 1L,M, S1D-G). By contrast, for V5-ZO1b-Alpha, none of the injected embryos expressed detectable V5-ZO1b-Alpha, even though 100% of sibling fish were successfully targeted as determined by PCR analysis (Fig. S1C). For V5-ZO1b-Beta, we generated a transgenic line (*V5-tjp1b-Beta*^{b1406}*)* and found V5 staining localized at puncta throughout the nervous system, generally colocalized with neural Connexins (Fig. S1H). Within the Mauthner circuit, neuronal GJs at both CEs and M/CoLo synapses are made of heterotypic channels formed by Cx35.5, encoded by the gene *gap junction delta 2a* (*gjd2a*), and Cx34.1, encoded by *gjd1a*, both homologous to mammalian Cx36 (*gjd2*) – both of these Connexins are recognized by the antibody against human Cx36 (Miller et al., 2017). We observed clear localization of V5-ZO1b-Beta to the stereotyped locations of CE and M/CoLo electrical synapses, colocalizing with neuronal Cx36 staining at the synaptic contacts (Fig. 1L, Fig. S1H). We conclude that both V5-ZO1b-Beta and V5-ZO1b-Gamma are localized to Mauthner electrical synapses.

ZO1b-Beta is necessary for robust Connexin localization to electrical synapses

The protein sequences predicted from the three *tjp1b/ZO1b* transcripts identify unique N-terminal peptide sequences for each, though only ZO1b-Alpha has an identifiable domain, a caspase activation and recruitment domain (CARD), while ZO1b-Beta and ZO1b-Gamma have sequences that fail to predict function including lipid modifications

found in PSD MAGUK isoforms (Fig. 1C, Fig. S2A). The common portion of all isoforms, however, retains the PDZ1 binding domain that we previously demonstrated mediates direct biochemical interaction with Cx34.1 (Fig. 1C). We first asked whether differential N-terminal sequences would affect Cx34.1 binding by cloning full-length sequences of *tjp1b/ZO1b-Alpha, tjp1b/ZO1b-Beta and tjp1b/ZO1b-Gamma* and used heterologous expression to test for interactions. HEK293T cells were co-transfected with individual ZO1b isoforms and full-length Cx34.1. Using western blot analysis with antibodies specific to ZO1b and Cx34.1, we found Cx34.1 was detected in all ZO1b isoform immune complexes compared to control immunoprecipitate (Fig. S2B). We conclude that zebrafish Cx34.1 can interact with each unique ZO1b isoform.

Next, we examined the role of each ZO1 isoform at electrical synapses using CRISPR/Cas9-induced mutations to knock out each individual isoform (CRISPR sites identified in Fig. 1A). For each isoform, we generated a mutant line and analyzed Cx35.5, Cx34.1, and ZO1 antibody staining at Mauthner circuit electrical synapses using immunohistochemistry (Fig. 2A-J). *tjp1b/ZO1b-beta*$^{-/-}$ mutants had a nearly complete reduction of both Cx35.5 and Cx34.1, as well as ZO1 staining, at both CE and M/CoLo synapses (Fig. 2G,H). Quantitation of Cx34.1 at M/CoLo contacts confirmed that staining was greatly diminished in *tjp1b/ZO1b-beta*$^{-/-}$ mutants compared to *wt* and other single isoform mutants (Fig. 2K). Using qPCR we found that both the *Alpha* and *Gamma* isoforms were still expressed in the *tjp1b/ZO1b-beta*$^{-/-}$ mutants, and their expression was upregulated compared with *wt*, suggesting they were present but unable to compensate for the loss of the *Beta* isoform (Fig. S2C). Further, despite the fact that V5-ZO1b-Gamma protein localizes to electrical synapses, we found that the *tjp1b/ZO1b-gamma*$^{-/-}$ mutant had little effect on Connexin or ZO1 staining at Mauthner circuit synapses. As expected from the expression analysis, *tjp1b/ZO1b-alpha*$^{-/-}$ mutants had no effect on Connexin or ZO1 staining. We conclude that ZO1b-Beta is required for robust Connexin localization to electrical synapses.

While greatly diminished compared to wildtype fish, *tjp1b/ZO1b-beta*$^{-/-}$ mutants retained ~10% of Connexin localization at Mauthner electrical synapses as compared with a mutant that knocks out all isoforms, *tjp1b/ZO1b-pan*$^{-/-}$ (the mutation is in exon 5, which is shared in all transcripts, Fig. 1A). To determine if ZO1b-Gamma plays a role with ZO1b-Beta at M/CoLo synapses, we generated *tjp1b/ZO1b-beta-gamma*$^{-/-}$ double mutants and quantitated the effect on Cx34.1 staining. Note that we generated the Gamma-disrupting mutation on the *ZO1b-beta* mutant chromosome (i.e., both the *beta* and *gamma* exons of the same *tjp1b* gene had CRISPR-induced disruptions), grew a line of animals, then analyzed double homozygous mutants that disrupted both the Beta and Gamma isoforms (see Methods). In *ZO1b-beta-gamma*$^{-/-}$ double mutants, there was a further loss of synaptic Cx34.1 staining (~46%) as compared to *tjp1b/ZO1b*$^{-/-}$*-beta* alone (Fig. 2K inset box), indicating that ZO1b-Gamma may play a minor role in scaffolding Connexins at electrical synapses. Taken together, we conclude that ZO1b-Beta and ZO1b-Gamma are localized to electrical synapses, yet the Beta isoform is differentially required for the robust localization of both Cx35.5 and Cx34.1 at synaptic contacts.

ZO1b-Beta is sufficient for robust Connexin localization to electrical synapses

Next, we examined whether the presence of ZO1b-Beta was sufficient for robust electrical synapse formation. To achieve this we generated *alpha-gamma* double mutants, on the same chromosome, leaving the *Beta* isoform intact. In *tjp1b/ZO1b-alpha-gamma*$^{-/-}$ double mutants, Cx35.5, Cx34.1 and ZO1 were robustly localized to CE and M/CoLo synapses as compared with wildtype fish (Fig. 3). From these observations we conclude that the presence of ZO1b-Beta is sufficient for robust Connexin localization to electrical synapses. Taken together, we provide evidence that both ZO1b-Beta and ZO1b-Gamma are localized to electrical synapses, yet the Beta isoform appears to have a special function in licensing Connexin localization to the synapse.

The results here reveal that ZO1b-Beta is the dominant isoform functioning to localize Connexins to electrical synapses, while ZO1b-Gamma is present it appears to have only a minor role. How this differential effect occurs is not understood. It could be due to the levels of isoform expression, with Beta being present at greater concentration at the electrical synapse as compared to Gamma. While we observed each ZO1b isoform at electrical synapses using the V5 tag, comparing their relative levels would require unique detection reagents. Our efforts at tagging electrical synapse proteins with alternative epitope tags (e.g., FLAG, HA, etc) has to date not been successful, so we are currently unable to compare the relative isoform levels at electrical synapses. Alternatively, rather than expression level differences, the unique amino acids of each isoform may impart distinct functions. At chemical synapses, unique scaffold isoforms encoded by single genes have been shown to play discrete functions in synapse development, neurotransmitter receptor localization, and plasticity (Araki et al., 2020; Goodman et al., 2017; Hirao et al., 2000). We envision that the Beta and Gamma isoforms may play unique roles at the electrical synapse. As shown here, ZO1b-Beta is necessary and sufficient for Connexin localization during development, while perhaps ZO1b-Gamma could be used to modulate an alternative function, such as electrical synapse plasticity (Arroyo et al., 2016; Bhattacharya et al., 2019; Bloomfield and Völgyi, 2009; Marder, 1998; Miller and Pereda, 2017). While no role for ZO1b-Alpha was observed in the formation of Mauthner electrical synapses under the conditions we tested, its unique N-terminal CARD domain may suggest specialized deployment to regulate apoptotic events or immune responses (Bouchier-Hayes and Martin, 2002). Future experiments that reveal the relative contributions of each isoform, and that further probe electrical synapse transmission, will reveal how the complexity of multiple ZO1b isoforms at the electrical synapse regulate structure and function.

Our recent work reveals that ZO1b is an exclusively postsynaptic member of the ESD, where it binds Connexins, and is necessary and sufficient for channel localization and function (Lasseigne et al., 2021). The previous work highlighted the hierarchical organization of electrical synapse formation, where a postsynaptic scaffold was required for the localization of the postsynaptic Connexin, yet the scaffold localized to the synapse independent of the Connexins. Such hierarchical relationships of structure and function are well appreciated at chemical synapses, yet these ideas are just emerging at electrical synapses (Lasseigne et al., 2021; Palumbos et al., 2021). A major barrier in the field is the lack of knowledge surrounding the proteomic makeup of the ESD, and the molecular mechanisms of molecules functioning in building electrical synapses. Our

working model is that ESD complexity comprises multiple unique classes of proteins, including cell adhesion, scaffolds, and regulatory molecules, all contributing to electrical synapse structure, function, and plasticity (Miller and Pereda, 2017). Our findings here reveal that we must further consider unique isoforms of each of the proteins identified at the ESD. Though we only investigated ZO1b isoforms resulting from alternative transcriptional initiation, there are many predicted alternatively spliced forms of downstream exons, many altering the protein-protein interaction domains, that could lead to additional scaffold complexity from this individual gene. Thus, we expect that ESD complexity will be derived from both discrete classes of molecules as well as unique protein isoforms of the same gene, each with distinct impacts on electrical synapse formation, function, and plasticity.

Materials and Methods

Zebrafish

Fish were maintained in the University of Oregon fish facility with approval from the Institutional Animal Care and Use Committee (IACUC AUP 21-42). Zebrafish, *Danio rerio*, were bred and maintained at 28°C on a 14 hr on and 10 hr off light cycle. Animals were housed in groups, generally of 25 animals per tank. Development time points were assigned via standard developmental staging (Kimmel et al., 1995). All fish used for this project were maintained in the ABC background developed at the University of Oregon. Most fish had the enhancer trap transgene *zf206Et (M/CoLo:GFP)* in the background (C. Satou et al., 2009), unless otherwise noted. The *V5-tjp1b-Beta*^{b1406} line contains an in-frame NH_2-V5 affinity tag in the *tjp1b Beta* gene (Lasseigne et al., 2021). The *tjp1b-pan*^{b1370} mutant line contains a 16 bp deletion in the *tjp1b* gene (common Exon 5, affecting all isoforms) (Marsh et al., 2017). The *tjp1b-alpha*^{b1429} mutant line contains an 8 bp deletion in the *tjp1b Alpha* first exon. The *tjp1b-beta*^{b1430} mutant line contains a 16 bp insertion in the *tjp1b Beta* first exon. The *tjp1b-gamma*^{b1431} mutant line contains a 7 bp deletion in the *tjp1b Gamma* first exon. The *tjp1b-gamma-beta*^{b1433} double mutant line contains an 11 bp deletion in the *tjp1b-Gamma* and a 16 bp insertion in the *tjp1b-Beta* first exons on the same chromosome. The *tjp1b-alpha-gamma*^{b1434} double mutant line contains a 4 bp deletion in the *tjp1b-Alpha* and an 8 bp deletion in the *tjp1b-Gamma* first exons on the same chromosome. Mutant lines were genotyped for all experiments. All immunohistochemistry and *in situ* analyses were performed at 5 dpf. At this stage of development, zebrafish sex is not yet determined (Wilson et al., 2014).

Cas9-mediated genome engineering of tjp1b/ZO1b isoform mutants

A single guide RNA (sgRNA) targeting isoform specific Exon 1 of the endogenous *tjp1b-alpha*, *tjp1b-beta*, and *tjp1b-gamma* coding sequence were designed using the CRISPRscan algorithm (Moreno-Mateos et al., 2015) and synthesized as previously described (Shah et al., 2015) using the T7 megascript kit (ThermoFisher). Sequences for sgRNA are as follows: *tjp1b Alpha,* 5'-AATTAATACGACTCACTATAGGGCGGGAGGAGGAATAAACGTTTTAGAGCTAGAAATAGCAAGTTAAAATAAGGCTAGTCCGTTATCAACTTGAAAAAGTGGCACCGAGTCGGTGCGGATC-3'; *tjp1b Beta,* 5'-AATTAATACGACTCACTATAGGTTTCTGGGAGGCAGGCTAGTTTTAGAGCTAGAAA

TAGCAAGTTAAAATAAGGCTAGTCCGTTATCAACTTGAAAAAGTGGCACCGAGTCG
GTGCGGATC-3'; and *tjp1b Gamma,* 5'-
AATTAATACGACTCACTATAGGCCCGGGCTGCCTCTAATAGTTTTAGAGCTAGAAA
TAGCAAGTTAAAATAAGGCTAGTCCGTTATCAACTTGAAAAAGTGGCACCGAGTCG
GTGCGGATC -3'.

Injection mixes were prepared in a pH 7.5 buffer solution of 300 mM KCl and 4 mM HEPES and contained a final concentration of 200 pg/nL sgRNA and 1600 pg/nL Cas9 protein (IDT). Injection mixes were incubated at 37 °C for 5 min immediately prior to injection to promote formation of the Cas9 and sgRNA complex. Embryos containing the enhancer trap transgene *zf206Et (M/CoLo:GFP)* were injected with 1nL at the one-cell stage (Burger et al., 2016). Injected embryos were raised to adulthood and outcrossed to wild-type animals. Animals carrying gene-disrupting mutations were identified and verified using PCR and Sanger sequencing. Generating double mutant lines required disrupting each gene on the same chromosome. To generate the *tjp1b-gamma-beta*^{b1433} double mutant line, we injected sgRNA targeting isoform specific Exon 1 of the endogenous *tjp1b-gamma* into 1-cell stage embryos derived from the *tjp1b-beta*^{b1430} mutant line. To generate the *tjp1b-alpha-gamma*^{b1434} double mutant line, we injected sgRNA targeting isoform specific Exon 1 of the endogenous *tjp1b-gamma* into 1-cell stage embryos derived from the *tjp1b-alpha*^{b1429} mutant line.

Cas9-mediated genome engineering of V5-tjp1b/ZO1b isoform mosaics
The *V5-tjp1b* isoform-specific single stranded donor oligos (ssODN) were designed to repair into the respective endogenous *tjp*1b loci. The ssODN contained ~40 bp homology arms which flanked an XbaI restriction site, V5 sequence, and a 5x glycine linker. If the inserted sequence did not disrupt the endogenous sgRNA recognition site, mutations were designed in the CRISPR/PAM sites of the ssODN to prevent further double stranded breaks after repair. The N-terminal CRISPR target sequences for each isoform are as follows: Alpha: 5'-TTGTGACAGCCCGAGTGTTTGGG-3'; Beta: 5'-GTATTTCTGGTAATTCACCA-3'; and Gamma: 5'-TGCCCGGGCTGCCTCTAATAAGG-3'. Sequences for synthesized sgRNA are as follows: Alpha: 5'-
AATTAATACGACTCACTATAGGGCTCTTGTCTGTCTTTGGGTTTTAGAGCTAGAAAT
AGC-3'; Beta: 5'-
AATTAATACGACTCACTATAGGATTTCTGGTAATTCACCAGTTTTAGAGCTAGAAAT
AGC-3'; and Gamma: 5'-
AATTAATACGACTCACTATAGGCCCGGGCTGCCTCTAATAGTTTTAGAGCTAGAAA
TAGC-3'. The sequences for the ssODN used for repair for each *tjp1b* isoform is as follows: Alpha: 5'-Alt-HDR-Modified-
CAAAAATTGCACAGAAATGACCACAAGTCTCTTCTAAAACATGTCTAGAGGCAAAC
CGATTCCGAACCCGCTGCTGGGCCTGGATAGCACCGGAGGTGGAGGCGGACTGC
TGTCAGTGTTCGGGGGACCTGTTGAAGAAGTGTTAGCAGGACTCCTCAAGCTGAA
G-Alt-Modified-3'; Beta: 5-
TGCGGATTTTTGTGTTTCAAAAAAGCGGTGAACAGTACCATGTCTAGAGGCAAACC
GATTCCGAACCCGCTGCTGGGCCTGGATAGCACCGGAGGTGGAGGCGGAGTGAA
TTACCAGAAATACATTACTGTTATGCAGCTGGCTC-3'; and Gamma: 5'-Alt-HDR-Modified-

CTCAACTTGCCTCGGCGCGAGCAGCTAAAGGAACAAAATGTCTAGAGGCAAACCG
ATTCCGAACCCGCTGCTGGGCCTGGATAGCACCGGAGGTGGAGGCGGATCAGCG
CGCGCAGCGTCTAATAAGGTTTGTGCTCATTTATACACATCTCAGACGCATTGTCT
GCAGTTGTCAG-Alt-Modified-3'

Injection mixes were prepared in a pH 7.5 buffer solution of 300 mM KCl and 4 mM HEPES and contained a final concentration of 2uM ssODN, 2.5-5uM sgRNA, and 8uM Cas9 protein (IDT) and were injected as described above. At 3 dpf, injected embryos were screened by PCR for integration of the isoform-specific ssODN repair template into the respective *tjp1b* locus using a forward primer against the V5 sequence (5'-CGATTCCGAACCCGCTGCTG-3') and an isoform-specific reverse primer. Isoform-specific primer sequences are as follows: Alpha: 5'-TCCAAGAAGAGCTCAGCACG-3'; Beta: 5'-AACCAAAAATGACACGACAGGCTTTCC-3'; Gamma: 5'-ACCGCACATATCGACTAGCG-3'. At 5 dpf, injected larvae were screened by immunohistochemistry for expression of V5-tjp1b isoforms.

Immunohistochemistry and confocal imaging

Anesthetized, 5 dpf larvae were fixed for 3 hr in 2% trichloroacetic acid in PBS (Martin et al., 2022). Fixed tissue was washed in PBS containing 0.5% Triton X-100, followed by standard blocking and antibody incubations. Primary antibody mixes included combinations of the following: rabbit anti-Cx35.5 (Fred Hutch Antibody Technology Facility, clone 12H5, 1:800), mouse IgG2A anti-Cx34.1 (Fred Hutch Antibody Technology Facility, clone 5C10A, 1:350), mouse IgG1 anti-ZO1 (Invitrogen, 33–9100, 1:350), mouse IgG2a anti-V5 (Invitrogen, R960-25, 1:500), rabbit anti-human Cx36 (Invitrogen, 36-4600, 1:500) and chicken anti-GFP (Abcam, ab13970, 1:350-1:500). All secondary antibodies were raised in goat (Invitrogen, conjugated with Alexa-405-Plus, –488, −555, or −633 fluorophores, 1:500). Tissue was then cleared stepwise in a 25%, 50%, 75% glycerol series, dissected, and mounted in ProLong Gold antifade reagent (ThermoFisher). Images were acquired on a Leica SP8 Confocal using a 405-diode laser and a white light laser set to 499, 553, 598, and 631 nm, depending on the fluorescent dye imaged. Each laser line's data was collected sequentially using custom detection filters based on the dye. Images of the Club Endings (CEs) were collected using a 63x, 1.40 numerical aperture (NA), oil immersion lens, and images of M/Colo synapses were collected using a 40x, 1.20 NA, water immersion lens. For each set of images, the optimal optical section thickness was used as calculated by the Leica software based on the pinhole, emission wavelengths, and NA of the lens. Within each experiment where fluorescence intensity was to be quantified, all animals were stained together using the same antibody mix, processed at the same time, and all confocal settings (laser power, scan speed, gain, offset, objective, and zoom) were identical. Multiple animals per genotype were analyzed to account for biological variation. To account for technical variation, fluorescence intensity values for each region of each animal were an average across multiple synapses.

Analysis of confocal imaging

For fluorescence intensity quantitation, confocal images were processed and analyzed using FiJi (Schindelin et al., 2012) software. To quantify staining at M/Colo synapses, a

standard region of interest (ROI) surrounding each M/CoLo site of contact was drawn, and the mean fluorescence intensity was measured. Standard deviations and errors were computed using Prism (GraphPad) software. Figure images were created using FiJi, Photoshop (Adobe), and Illustrator (Adobe). Statistical analyses were performed using Prism (GraphPad) and unpaired t-test with Welch's correction was performed. For all experiments, values were normalized to *wildtype* control animals unless otherwise noted, and n represented the number of fish used.

scRNA-seq analysis

The full methods from the embryo dissociation, DNA library preparation, sequencing, and bioinformatic method can be found from the original dataset publication (Farnsworth et al., 2020). In short, whole larvae from the Tg(olig2:GFP)vu12 and Tg(elavl3:GCaMP6s) backgrounds were pooled (n=15 per replicate), with 2 replicates at each timepoint (1, 2, 5dpf). Dissociated cells were then run on a 10X Chromium platform using 10x v.2 chemistry aiming for 10,000 cells per run. We aligned reads to the zebrafish genome, GRCz11, using the 10X Cellranger pipeline (version 3.1) using the Lukowicz-Bedford GTF (Lukowicz-Bedford et al., 2022), which incorporates genome wide improvements (Lawson et al., 2020). Transcriptomes were analyzed using the Seurat (V3.1.5) software package for R (V4.1.0) using standard quality control, normalization, and analysis steps. Final UMAP analysis resulted in 49,367 cells with 115 PC dimensions and a resolution of 15.0, which produced 238 clusters. Resources can be found at www.adammillerlabcom/resources.

Fluorescent RNA *in situ*

Custom RNAscope probes to target isoform-specific *tjp1b* genes were designed and ordered through ACD. For fluorescent *in situs*, we used a modified RNAscope protocol (Gross-Thebing et al., 2014). Briefly, 5 dpf embryos were fixed for 1 h at room temperature in 4% paraformaldehyde (PFA)/ 4% sucrose, rinsed in PBS/0.1% Tween20, dehydrated through a methanol series and then stored in 100% methanol at −20°C at least overnight. The methanol was removed, and the tissue was air dried for 30 min at room temperature. The tissue was then exposed to Protease Plus for 1 hr 15 min and washed with PBS/0.1% Tween 20. The probe was pre-warmed at 40 °C, then cooled. Tissue was incubated with probe overnight at 40 °C. Standard RNAscope V2 multiplex reagents and Opal fluorophores were used, with the modification that 0.2X SSC/0.1% Tween 20 was used for all wash steps. After in situ, tissue was rinsed in PBS/0.1% Tween 20, then immunostained as described above with the exception that Tween 20 was used as the detergent instead of Triton X-100. Stained tissue was either mounted (whole mount) and imaged in 75% glycerol or dissected and mounted with ProLong Gold Antifade.

Cell culture, transfection, and immunoprecipitation

HEK293T/17 verified cells were purchased from ATCC (CRL-11268; STR profile, amelogenin: X). Cells were expanded and maintained in Dulbecco's Modified Eagle's Medium (DMEM, ATCC) plus 10% fetal bovine serum (FBS, Gibco) at 37 °C in a humidified incubator in the presence of 5% CO_2. Low passage aliquots were cryopreserved and stored according to manufacturer's instructions. Cells from each

thawed cryovial were monitored for mycoplasma contamination using the Universal Mycoplasma Detection Kit (ATCC, 30–1012K).

ZO1b-Alpha and ZO1b-Beta were cloned into the pCMV expression vector with an NH_2-terminal mVenus tag and a COOH-terminal 8xHIS tag. ZO1b-Gamma was cloned into the pCMV expression vector with a COOH-terminal 8xHIS tag. Cx34.1 was expressed from a pCMV vector generated in a previous study (Lasseigne et al., 2021). Low passage HEK293T/17 cells were seeded 24 hr prior to transfection (1×10^6 cells/well of a six-well dish), and the indicated plasmids were co-transfected using Lipofectamine 3000 (Invitrogen) following the manufacturer's instructions. Cells were collected 36–48 hr post-transfection and lysed in 0.25 ml solubilization buffer (50 mM Tris [pH7.4], 100 mM NaCl, 5 mM EDTA, 1.5 mM MgCl2, 1 mM DTT and 1% Triton X-100) plus a protease inhibitor cocktail (Pierce). Lysates were centrifuged at 20,000 x g for 30 min at 4°C, and equal amounts of extract were immunoprecipitated with 1.0 µg mouse anti-ZO1 (Invitrogen, 33–9100) overnight with rocking at 4°C. Immunocomplexes were captured with 25 µl prewashed Protein A/G agarose beads for 1 hr with rocking at 4 °C. Beads were washed three times with lysis buffer, and bound proteins were boiled for 3 min in the presence of LDS-PAGE loading dye containing 200 mM DTT. Samples were resolved by SDS-PAGE using a 4–15% gradient gel and analyzed by Western blot using the following primary antibodies: mouse anti-ZO1 (Invitrogen, 33–9100) and rabbit anti-Cx34.1 3A4 (Fred Hutch Antibody Technology Facility, clone 3A4). Compatible near-infrared secondary antibodies were used for visualization with the Odyssey system (LI-COR).

qPCR analysis

RNA was isolated from 5 dpf larvae using TRIzol reagent, and 5 µg total RNA was used to synthesize cDNA using the Superscript III First strand cDNA synthesis kit (ThermoFisher). qPCR was performed using BioRad CFX Opus 96 Real-Time PCR System thermocycler using the SSsoAdvanced Universal SYBR® Green Supermix (BioRad) per manufacturer's instructions. All samples were performed in technical triplicate over three independent experiments.

Primers were designed to bind around intron/exon boundaries and to amplify *tjp1b/ZO1b* isoforms. Sequences are as follows: *tjp1b/ZO1b-alpha*, 5'-TGCTGGAGGAGGTGTGT-3' and 5'-CTGTGCGCTGGTTTAGTTTG-3' (exon 1 Alpha-exon 2); *tjp1b/ZO1b-beta,* 5'-CTGTTATGCAGCTGGCTCTA-3' and 5'-AACTGCAGGGCCGTATTT-3' (exon 1 Beta -exon 3); *tjp1b/ZO1b-gamma, 5'*-CCCGGGCTGCCTCTAATA-3' and 5'-CCTGTGTAGAGTTACAGTGTGC-3' (exon 1 Gamma-exon 5); and reference gene *eef1a1*, 5'-ATGGCACGGTGACAACAT-3' and 5'ATGGCACGGTGACAACAT-3'.

Acknowledgments

We would like to thank and acknowledge the University of Oregon zebrafish facility staff for superb fish care, especially through the challenges of the global pandemic. We would like to thank the administrative staff at the University of Oregon Institute of Neuroscience.

Competing Interests
None to declare.

Funding
The Developmental Biology Training Program, NICHD, T32HD007348 supported LEK and the Graduate Training in Genetics program, NIGMS, T32GM007413 supported RML. Eunice Kennedy Shriver National Institute of Child Health and Human Development F32HD102182 supported E.A.M. NINDS R21NS117967 and R01NS105758 to A.C.M.

References

Ackermann F, Waites CL, Garner CC. 2015. Presynaptic active zones in invertebrates and vertebrates. *EMBO Rep* **16**:923–938. doi:10.15252/embr.201540434

Araki Y, Hong I, Gamache TR, Ju S, Collado-Torres L, Shin JH, Huganir RL. 2020. SynGAP isoforms differentially regulate synaptic plasticity and dendritic development. *Elife* **9**. doi:10.7554/eLife.56273

Arroyo DA, Kirkby LA, Feller MB. 2016. Retinal Waves Modulate an Intraretinal Circuit of Intrinsically Photosensitive Retinal Ganglion Cells. *Journal of Neuroscience* **36**:6892–6905. doi:10.1523/JNEUROSCI.0572-16.2016

Bartelmez GW, Hoerr NL. 1933. The vestibular club endings in ameiurus. Further evidence on the morphology of the synapse. *The Journal of Comparative Neurology* **57**:401–428.

Bhattacharya A, Aghayeva U, Berghoff EG, Hobert O. 2019. Plasticity of the Electrical Connectome of C. elegans. *Cell* **176**:1174-1189.e16. doi:10.1016/j.cell.2018.12.024

Bloomfield SA, Völgyi B. 2009. The diverse functional roles and regulation of neuronal gap junctions in the retina. *Nature Reviews Neuroscience* **10**:495–506. doi:10.1038/nrn2636

Bouchier-Hayes L, Martin SJ. 2002. CARD games in apoptosis and immunity. *EMBO Rep* **3**:616–621. doi:10.1093/embo-reports/kvf139

Brightman MW, Reese TS. 1969. JUNCTIONS BETWEEN INTIMATELY APPOSED CELL MEMBRANES IN THE VERTEBRATE BRAIN. *Journal of Cell Biology* **40**:648–677. doi:10.1083/jcb.40.3.648

Burger A, Lindsay H, Felker A, Hess C, Anders C, Chiavacci E, Zaugg J, Weber LM, Catena R, Jinek M, Robinson MD, Mosimann C. 2016. Maximizing mutagenesis with solubilized CRISPR-Cas9 ribonucleoprotein complexes. *Development*. doi:10.1242/dev.134809

Eaton RC, Farley RD, Kimmel CB, Schabtach E. 1977. Functional development in the Mauthner cell system of embryos and larvae of the zebra fish. *J Neurobiol* **8**:151–172. doi:10.1002/neu.480080207

Farnsworth DR, Saunders LM, Miller AC. 2020. A single-cell transcriptome atlas for zebrafish development. *Developmental Biology* **459**:100–108. doi:10.1016/j.ydbio.2019.11.008

González-Mariscal L, Betanzos A, Ávila-Flores A. 2000. MAGUK proteins: structure and role in the tight junction. *Seminars in Cell & Developmental Biology* **11**:315–324. doi:10.1006/scdb.2000.0178

Goodman L, Baddeley D, Ambroziak W, Waites CL, Garner CC, Soeller C, Montgomery JM. 2017. N-terminal SAP97 isoforms differentially regulate synaptic structure and postsynaptic surface pools of AMPA receptors. *Hippocampus* **27**:668–682. doi:10.1002/hipo.22723

Grant SGN. 2019. Synapse diversity and synaptome architecture in human genetic disorders. *Human Molecular Genetics* **28**:R219–R225. doi:10.1093/hmg/ddz178

Gross-Thebing T, Paksa A, Raz E. 2014. Simultaneous high-resolution detection of multiple transcripts combined with localization of proteins in whole-mount embryos. *BMC Biology* **12**:55. doi:10.1186/s12915-014-0055-7

Hirao K, Hata Y, Yao I, Deguchi M, Kawabe H, Mizoguchi A, Takai Y. 2000. Three Isoforms of Synaptic Scaffolding Molecule and Their Characterization. *Journal of Biological Chemistry* **275**:2966–2972. doi:10.1074/jbc.275.4.2966

Jacoby J, Kimmel CB. 1982. Synaptogenesis and its relation to growth of the postsynaptic cell: a quantitative study of the developing Mauthner neuron of the axolotl. *J Comp Neurol* **204**:364–376.

Kimmel CB, Ballard WW, Kimmel SR, Ullmann B, Schilling TF. 1995. Stages of embryonic development of the zebrafish. *Developmental Dynamics* **203**:253–310. doi:10.1002/aja.1002030302

Lafarga M, Tapia O, Romero AM, Berciano MT. 2017. Cajal bodies in neurons. *RNA Biology* **14**:712–725. doi:10.1080/15476286.2016.1231360

Lasseigne AM, Echeverry FA, Ijaz S, Michel JC, Martin EA, Marsh AJ, Trujillo E, Marsden KC, Pereda AE, Miller AC. 2021. Electrical synaptic transmission requires a postsynaptic scaffolding protein. *Elife* **10**. doi:10.7554/eLife.66898

Lawson ND, Li R, Shin M, Grosse A, Yukselen O, Stone OA, Kucukural A, Zhu L. 2020. An improved zebrafish transcriptome annotation for sensitive and comprehensive detection of cell type-specific genes. *Elife* **9**. doi:10.7554/eLife.55792

Liu KS, Fetcho JR. 1999. Laser Ablations Reveal Functional Relationships of Segmental Hindbrain Neurons in Zebrafish. *Neuron* **23**:325–335.

Lukowicz-Bedford RM, Farnsworth DR, Miller AC. 2022. Connexinplexity: the spatial and temporal expression of *connexin* genes during vertebrate organogenesis. *G3 Genes|Genomes|Genetics* **12**. doi:10.1093/g3journal/jkac062

Marder E. 1998. Electrical synapses: Beyond speed and synchrony to computation. *Current Biology* **8**:R795–R797. doi:10.1016/S0960-9822(07)00502-7

Marsh AJ, Michel JC, Adke AP, Heckman EL, Miller AC. 2017. Asymmetry of an Intracellular Scaffold at Vertebrate Electrical Synapses. *Current Biology* **27**:3561-3567.e4. doi:10.1016/j.cub.2017.10.011

Martin E, Ijaz S, Pereda A, Miller A. 2022. Trichloroacetic Acid Fixation and Antibody Staining of Zebrafish Larvae. *BIO-PROTOCOL* **12**. doi:10.21769/BioProtoc.4289

Martin EA, Lasseigne AM, Miller AC. 2020. Understanding the Molecular and Cell Biological Mechanisms of Electrical Synapse Formation. *Frontiers in Neuroanatomy* **14**. doi:10.3389/fnana.2020.00012

Miller AC, Pereda AE. 2017. The electrical synapse: Molecular complexities at the gap and beyond. *Developmental Neurobiology* **77**:562–574. doi:10.1002/dneu.22484

Miller AC, Voelker LH, Shah AN, Moens CB. 2015. Neurobeachin is required postsynaptically for electrical and chemical synapse formation. *Current Biology* **25**:16–28. doi:10.1016/j.cub.2014.10.071

Miller AC, Whitebirch AC, Shah AN, Marsden KC, Granato M, O'Brien J, Moens CB. 2017. A genetic basis for molecular asymmetry at vertebrate electrical synapses. *Elife* **6**. doi:10.7554/eLife.25364

Moreno-Mateos MA, Vejnar CE, Beaudoin J-D, Fernandez JP, Mis EK, Khokha MK, Giraldez AJ. 2015. CRISPRscan: designing highly efficient sgRNAs for CRISPR-Cas9 targeting in vivo. *Nature Methods* **12**:982–988. doi:10.1038/nmeth.3543

Moroz LL, Kohn AB. 2016. Independent origins of neurons and synapses: insights from ctenophores. *Philosophical Transactions of the Royal Society B: Biological Sciences* **371**:20150041. doi:10.1098/rstb.2015.0041

Palumbos SD, Skelton R, McWhirter R, Mitchell A, Swann I, Heifner S, von Stetina S, Miller DM. 2021. cAMP controls a trafficking mechanism that maintains the neuron specificity and subcellular placement of electrical synapses. *Developmental Cell* **56**:3235-3249.e4. doi:10.1016/j.devcel.2021.10.011

Pereda AE. 2014. Electrical synapses and their functional interactions with chemical synapses. *Nature Reviews Neuroscience* **15**:250–263. doi:10.1038/nrn3708

Pereda AE, Rash JE, Nagy JI, Bennett MVL. 2004. Dynamics of electrical transmission at club endings on the Mauthner cells. *Brain Res Brain Res Rev* **47**:227–244.

Ryan TJ, Grant SGN. 2009. The origin and evolution of synapses. *Nature Reviews Neuroscience* **10**:701–712. doi:10.1038/nrn2717

Satou Chie, Kimura Y, Kohashi T, Horikawa K, Takeda H, Oda Y, Higashijima S. 2009. Functional role of a specialized class of spinal commissural inhibitory neurons during fast escapes in zebrafish. *J Neurosci* **29**:6780–6793.

Satou C., Kimura Y, Kohashi T, Horikawa K, Takeda H, Oda Y, Higashijima S -i. 2009. Functional Role of a Specialized Class of Spinal Commissural Inhibitory Neurons during Fast Escapes in Zebrafish. *Journal of Neuroscience* **29**:6780–6793. doi:10.1523/JNEUROSCI.0801-09.2009

Schindelin J, Arganda-Carreras I, Frise E, Kaynig V, Longair M, Pietzsch T, Preibisch S, Rueden C, Saalfeld S, Schmid B, Tinevez J-Y, White DJ, Hartenstein V, Eliceiri K, Tomancak P, Cardona A. 2012. Fiji: an open-source platform for biological-image analysis. *Nature Methods* **9**:676–682. doi:10.1038/nmeth.2019

Shah AN, Davey CF, Whitebirch AC, Miller AC, Moens CB. 2015. Rapid reverse genetic screening using CRISPR in zebrafish. *Nature Methods* **12**:535–540. doi:10.1038/nmeth.3360

Siddiqui TJ, Craig AM. 2011. Synaptic organizing complexes. *Current Opinion in Neurobiology* **21**:132–143. doi:10.1016/j.conb.2010.08.016

Wilson CA, High SK, McCluskey BM, Amores A, Yan Y, Titus TA, Anderson JL, Batzel P, Carvan MJ, Schartl M, Postlethwait JH. 2014. Wild Sex in Zebrafish: Loss of the Natural Sex Determinant in Domesticated Strains. *Genetics* **198**:1291–1308. doi:10.1534/genetics.114.169284

Yao C, Vanderpool KG, Delfiner M, Eddy V, Lucaci AG, Soto-Riveros C, Yasumura T, Rash JE, Pereda AE. 2014. Electrical synaptic transmission in developing zebrafish. *J Neurophysiol* **0552827**:2102–13. doi:10.1152/jn.00397.2014

Zheng C-Y, Seabold GK, Horak M, Petralia RS. 2011. MAGUKs, Synaptic Development, and Synaptic Plasticity. *The Neuroscientist* **17**:493–512. doi:10.1177/1073858410386384
Zhu J, Shang Y, Zhang M. 2016. Mechanistic basis of MAGUK-organized complexes in synaptic development and signalling. *Nature Reviews Neuroscience* **17**:209–223. doi:10.1038/nrn.2016.18

Figure Legend:

Figure 1. Alternatively initiated isoforms *tjp1b/ZO1b-Beta* and *tjp1b/ZO1b-Gamma* are expressed in the Mauthner cell circuit and localize to electrical synapses. A. Schematic diagram of the *tjp1b/ZO1b* gene locus on chromosome 25: 32,031,536-32,271,394 (GRCz11 Ensembl) showing the exon structure located on the forward strand. Horizontal black bar represents the DNA strand and vertical black bars represent individual exons. The region containing alternatively initiated exons for *tjp1b/ZO1b-Alpha*, *-Beta*, and *-Gamma* isoforms is expanded between the dashed lines (Chromosome 25: 32,031,536-32,208,713). Unique initiation exons are represented by white boxes (Exons 1 Alpha, 1 Beta, and 1 Gamma), additional exons are represented by grey boxes, and the first shared exon is represented by a black box (Exon 5). Lengths of exons and introns are indicated. The CRISPR target sequences used to generate mutations to knock out isoform function are indicated (5'-to-3') in the expanded regions of unique Exons 1 Alpha, 1 Beta, and 1 Gamma and shared Exon 5 (Pan). PAM sequences are underlined. Note that the CRISPR target sequence for *tjp1b/ZO1b-beta* is on the reverse strand. **B.** Schematic diagram representing the alternatively initiated *tjp1b/ZO1b* isoform cDNAs *tjp1b/ZO1b-alpha* (ENSDART00000173656.2; 7618 bp), -*beta* (ENSDART00000155992.3; 7626 bp) and -*gamma* (ENSDART00000112588.5; 7408 bp). Unique 5'UTRs and initiation exons are represented by white boxes, additionally spliced exons are represented by grey boxes, and exons shared by all three isoforms are represented by black boxes (Exons 5-31). Approximate location of the ATG start codon and the shared TGA stop codon are indicated in each transcript. **C.** Schematic diagram of the ZO1b isoform proteins representing ZO1b-Alpha (2005 aa), -Beta (1853 aa), and -Gamma (1689 aa). The unique N-terminal amino acid sequences are indicated in the dashed box. Note that ZO1b-Alpha and ZO1b-Beta both contain amino acid sequence derived from exons 3 and 4. Domains are depicted as white shapes; CARD, PDZ, SH3, GUK and ZU5 are protein-protein interaction modules. White bars represent regions derived from unique initiation exons, grey bars represent regions derived from additionally spliced exons and black bars represent regions derived from shared exons. **D-K.** Confocal images of fluorescent RNA *in situ* (white) for the negative control *DapB* (**D, E**), *tjp1b/ZO1b-alpha* (**F, G**)*, tjp1b/ZO1b-beta* (**H, I**), and *tjp1b/ZO1b-gamma* (**J, K**) in the Mauthner circuit cell bodies of 5 dpf *zf206Et* zebrafish larvae from *wildtype* (*wt*). Animals are co-stained with anti-GFP (green). Scale bars = 2 µm. Images of the Mauthner cell body (D, F, H, J) are maximum intensity projections of ~15-30 µm. Boxed regions are enlarged in D', F', H' and J' and neighboring panels show individual channels. Images of the CoLo cell body (E, G, I, K) are maximum intensity projections of ~6-12 µm and neighboring panels show individual channels. The green dashed line in the probe channel indicates the outline of the CoLo cell body. In G,

the arrow indicates the *Alpha* signal in unidentified nearby cells. In H-K, the *Beta* and *Gamma* signal appears as distinct structures in the nucleus likely to be Cajal bodies (Lafarga et al., 2017). **L, M.** Confocal images of the sites of contact of Mauthner/CoLo processes in the spinal cord of 5 dpf zebrafish larvae from V5-tjp1b/ZO1b-Beta animals (**L**) and larvae mosaically expressing V5-tjp1b/ZO1b-Gamma (**M**). Animals are stained with anti-neurofilament (NF) (blue), anti-Cx36 (white), and anti-V5 (magenta). Scale bars = 2 µm. Boxed regions denote stereotyped location of electrical synapses and are enlarged in neighboring panels. Images are maximum-intensity projections of ~5 µm. In L' and M' images are from a single 0.3 µm Z-plane and the white dashed circle denotes the M/CoLo site of contact. Neighboring panels show individual channels.

Figure 2. ZO1b-Beta is necessary for robust Connexin localization to electrical synapses. A-J. Confocal images of Mauthner circuit neurons and stereotypical electrical synaptic contacts in 5 dpf *zf206Et* zebrafish larvae from *wt* (**A, B**), *tjp1b/ZO1b-pan*$^{-/-}$ (**C, D**), *tjp1b/ZO1b-alpha*$^{-/-}$ (**E, F**), *tjp1b/ZO1b-beta*$^{-/-}$ (**G, H**), and *tjp1b/ZO1b-gamma*$^{-/-}$ (**I, J**) animals. Animals are stained with anti-GFP (green), anti-Cx35.5 (cyan), anti-Cx34.1 (yellow), and anti-ZO1 (magenta). Scale bars = 2 µm. Boxed regions denote stereotyped location of electrical synapses and regions are enlarged in neighboring panels. Images of the Mauthner cell body and lateral dendrite in the hindbrain (A, C, E, G, I) are maximum intensity projections of ~10-20 µm. In A', C', E', G', and I', images are maximum-intensity projections of ~3-6 µm and neighboring panels show the individual channels. Images of the sites of contact of M/CoLo processes in the spinal cord (B, D, F, H, J) are maximum-intensity projections of ~6-8 µm. In B', D', F', H' and J', images are from a single 0.42 µm Z-plane and the white dashed circle denotes the location of the M/CoLo site of contact. Neighboring panels show individual channels. **K.** Quantification of Cx34.1 fluorescence intensities at M/CoLo synapses for the noted genotypes. The height of the bar represents the mean of the sampled data normalized to the *wt* average. Circles represent the normalized value of each individual animal. *wt* n=11; *tjp1b/ZO1b-pan*$^{-/-}$ n=3, p<0.0001; *tjp1b/ZO1b-alpha*$^{-/-}$ n=5, p=0.1005, ns; *tjp1b/ZO1b-beta*$^{-/-}$ n=5, p<0.0001; *tjp1b/ZO1b-gamma*$^{-/-}$ n=5, p=0.7453, ns. In K inset box, the height of the bar represents the mean of the sampled data normalized to the *tjp1b/ZO1b-beta*$^{-/-}$ average. Circles represent the normalized value of each individual animal. *tjp1b/ZO1b-beta*$^{-/-}$ n=6; *tjp1b/ZO1b-beta-gamma*$^{-/-}$, n=6 p=0.0023. Error bars are ± SEM.

Figure 3. ZO1b-Beta is sufficient for robust Connexin localization to electrical synapses. (A-D). Confocal images of Mauthner circuit neurons and stereotypical electrical synaptic contacts in 5 dpf *zf206Et* zebrafish larvae from *wt* (**A, B**) and *tjp1b/ZO1b-alpha-gamma*$^{-/-}$ double mutant (**C, D**) animals. Animals are stained with anti-GFP (green), anti-Cx35.5 (cyan), anti-Cx34.1 (yellow), and anti-ZO1 (magenta). Scale bars = 2 µm. Boxed regions denote stereotyped location of electrical synapses and regions are enlarged in neighboring panels. Images of the Mauthner cell body and lateral dendrite in the hindbrain (A, C) are maximum intensity projections of ~10-20 µm. In A' and C', images are maximum-intensity projections of ~3-6 µm and neighboring panels show the individual channels. Images of the sites of contact of M/CoLo processes in the spinal cord (B, D) are maximum-intensity projections of ~4-7 µm. In B'

and D', images are from a single 0.42 µm Z-plane and the white dashed circle denotes the location of the M/CoLo site of contact. Neighboring panels show individual channels.

Figure S1. Characterization of *tjp1b/ZO1b* isoform tissue expression. A. scRNA-seq dataset of *tjp1b/ZO1b* expression in early development where grey represents low expression and magenta represents the highest level of expression. Cells are derived from whole embryos at 1, 2, and 5 dpf and graphed together in UMAP space. Annotated cell types of clusters are indicated, and each dot represents a single cell. **B.** Confocal tile scan of fluorescent RNA *in situ* in whole 5 dpf *wt* zebrafish larvae for negative control *DapB*, *tjp1b/ZO1b-alpha, tjp1b/ZO1b-beta*, and *tjp1b/ZO1b-gamma*. Images are maximum intensity projections of ~68-98 µm. Contrast is inverted for clarity. Black arrowhead denotes signal in spinal cord. Black arrow denotes signal in hindbrain. While there is possible expression of all three isoforms in the vacuolar cells of the notochord compared with the negative control (blue arrowheads) and notochord expression as detected by scRNA-seq methods (Fig. S1A), we note that the fluorescent RNA *in situ* method often non-specifically detects signal in the notochord. Scale bar = 20 µm. **C.** Detection of V5-N-terminal tag integration by CRISPR/Cas9 mediated HDR using a short, single nucleotide repair oligo. Genomic DNA prepared from individual injected 5 dpf zebrafish was analyzed for successful integration by PCR using a forward primer against the V5 tag and a reverse primer outside the modified region. Products for V5-Alpha (top), V5-Beta (middle) and V5-Gamma (bottom) were resolved by agarose gel electrophoresis (indicated by black arrows). Non-specific products are indicated with an asterisk (*). U = uninjected siblings, NTC = no template control. The table shows the percentage of siblings positive for integration and the percentage of siblings positive for V5 immunostain, indicating mosaic expression of V5-tagged ZO1b isoforms. **D-G.** Confocal images of hindbrain and spinal cord in 5 dpf *wt* zebrafish larvae mosaically expressing V5-ZO1b-Gamma. Animals are stained with anti-NF (blue), anti-V5 (magenta), and anti-Cx36 (white). Scale bars = 2 µm. Boxed regions denote areas of V5-ZO1b Gamma staining and regions are enlarged in neighboring panels. **D.** Image of the hindbrain. Image is a maximum intensity projection of ~8 µm. Blue outline indicates the location of Mauthner cell body and lateral dendrites for anatomical orientation. In D', neighboring panels show individual channels. Note co-staining of Cx36 and V5-ZO1b-Gamma. **E-G.** Images of spinal cord. Images are maximum-intensity projections of ~7-16 µm. In E'-G', neighboring panels show individual channels. Note that Cx36 and V5-ZO1b-Gamma do not co-stain in these examples. **H.** Confocal tile scan of zebrafish brain from 5 dpf *zf206Et* zebrafish larvae from *V5-tjp1b/ZO1b-Beta* animals. Images are maximum intensity projections of ~42 µm. Animals are stained with anti-GFP (green), anti-V5 (magenta), and anti-Cx36 (white). Scale bars = 20 µm. Boxed region denotes stereotyped location of electrical synapses where V5-ZO1b-Beta and Cx36 overlap, and region is enlarged in neighboring panels. White arrows denote regions where V5-ZO1b-Beta and Cx36 do not overlap. Note orientation of anterior on left and posterior on right. In H', neighboring panels show individual channels.

Figure S2. Characterization of unique regions of ZO1b isoforms. A. Amino acid sequence alignment of unique N-termini from ZO1b isoforms. The grey box outlining amino acids in ZO1b-Alpha indicates the CARD protein-protein interaction domain. **B.**

ZO1b isoform interaction with Cx34.1. HEK293T/17 cells were transfected with plasmids to express Cx34.1 and empty vector (lane 1), ZO1b-Alpha (lane 2), ZO1b-Beta (lane 3), or ZO1b-Gamma (lane 4). Lysates were immunoprecipitated with anti-ZO1 antibody and analyzed by immunoblot for the presence of ZO1b isoform (upper) using anti-ZO1 antibody and Cx34.1 protein using Cx34.1-specific antibody (middle). Total extracts (bottom, 5% input) were blotted for Cx34.1 to demonstrate equivalent expression. Results are representative of three independent experiments. **C.** qPCR analysis of ZO1b isoform mRNA levels in *wt* and *tjp1b/ZO1b-beta*$^{-/-}$ mutants. Relative quantification of ZO1b isoform expression was determined after normalizing to a reference gene using the $2^{-\Delta\Delta C_T}$ (Livak) method. The height of the bar represents the relative gene expression in *tjp1b/ZO1b-beta*$^{-/-}$ mutants compared to *wt* for each *tjp1b/ZO1b* isoform, as labeled. Circles represent results of three independent experiments. Transcriptional upregulation of each isoform is observed. *wt* n=3; *tjp1b/ZO1b-alpha* n=3, p=0.0472; *tjp1b/ZO1b-beta* n=3, p=0.234; *tjp1b/ZO1b-gamma* n=3, p=0.232. Two-tailed unpaired t-test was used to calculate p values. Error bars are ± SEM.

Fig. 1

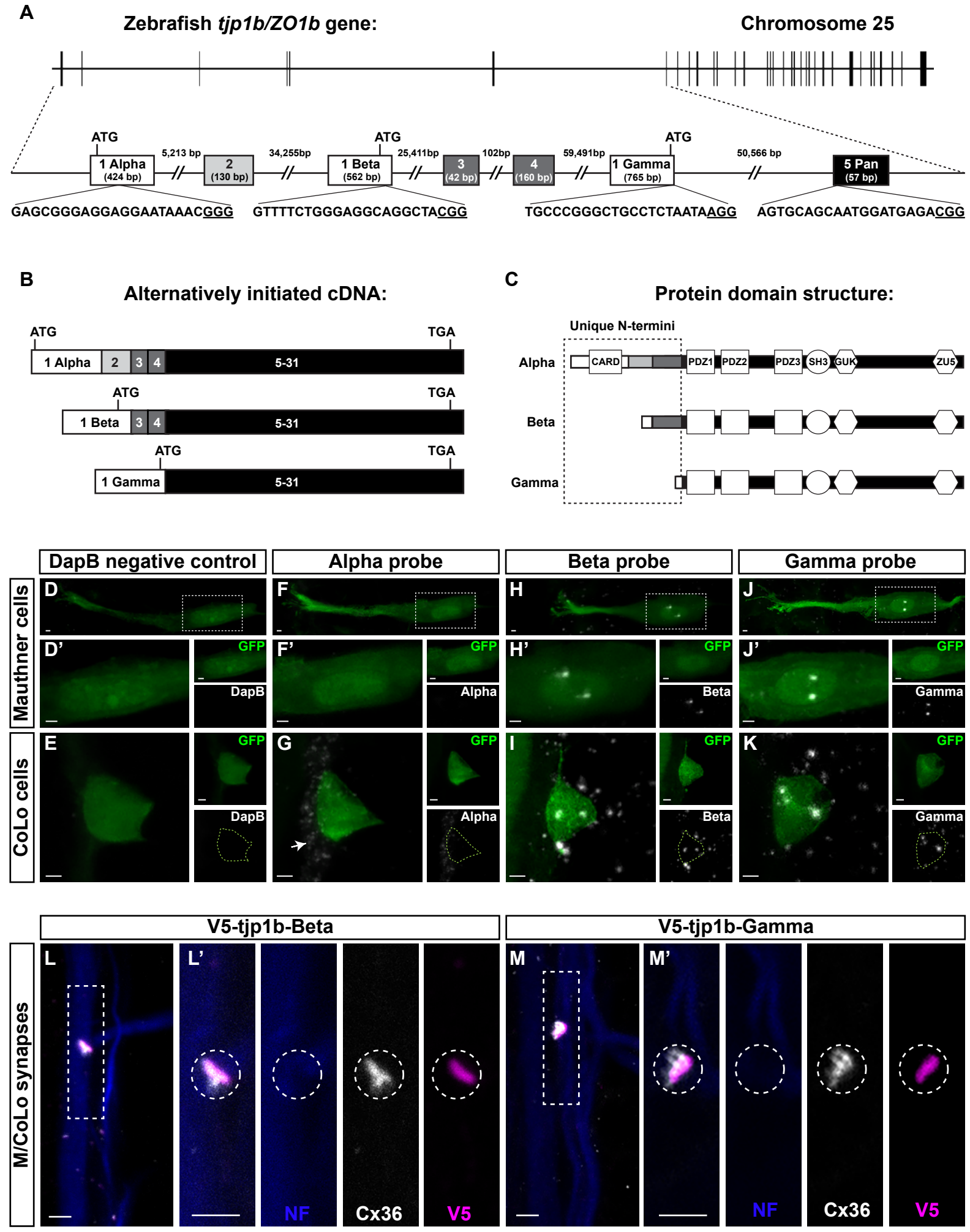
A
Zebrafish tjp1b/ZO1b gene:
Chromosome 25
ATG
1 Alpha (424 bp)
5,213 bp
2 (130 bp)
34,255bp
ATG
1 Beta (562 bp)
25,411bp
3 (42 bp)
102bp
4 (160 bp)
59,491bp
ATG
1 Gamma (765 bp)
50,566 bp
5 Pan (57 bp)
GAGCGGGAGGAGGAATAAACGGG
GTTTTCTGGGAGGCAGGCTACGG
TGCCCGGGCTGCCTCTAATAAGG
AGTGCAGCAATGGATGAGACGG
B
Alternatively initiated cDNA:
ATG
TGA
1 Alpha
2
3
4
5-31
1 Beta
1 Gamma
C
Protein domain structure:
Unique N-termini
Alpha
Beta
Gamma
CARD
PDZ1
PDZ2
PDZ3
SH3
GUK
ZU5
DapB negative control
Alpha probe
Beta probe
Gamma probe
Mauthner cells
CoLo cells
D
D'
E
F
F'
G
H
H'
I
J
J'
K
GFP
DapB
Alpha
Beta
Gamma
V5-tjp1b-Beta
V5-tjp1b-Gamma
M/CoLo synapses
L
L'
M
M'
NF
Cx36
V5

Fig. S1

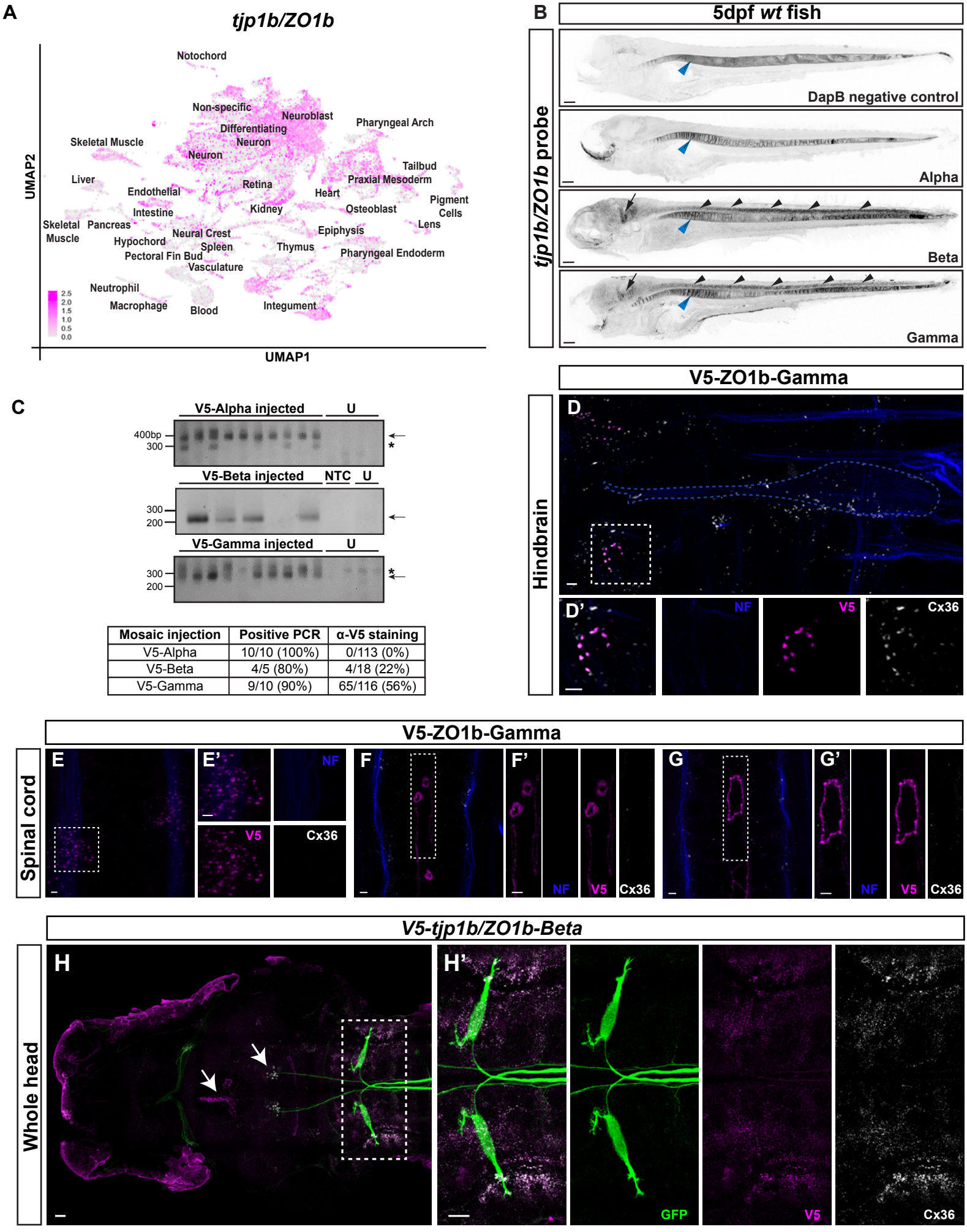

Mosaic injection	Positive PCR	α-V5 staining
V5-Alpha	10/10 (100%)	0/113 (0%)
V5-Beta	4/5 (80%)	4/18 (22%)
V5-Gamma	9/10 (90%)	65/116 (56%)

Fig. 2

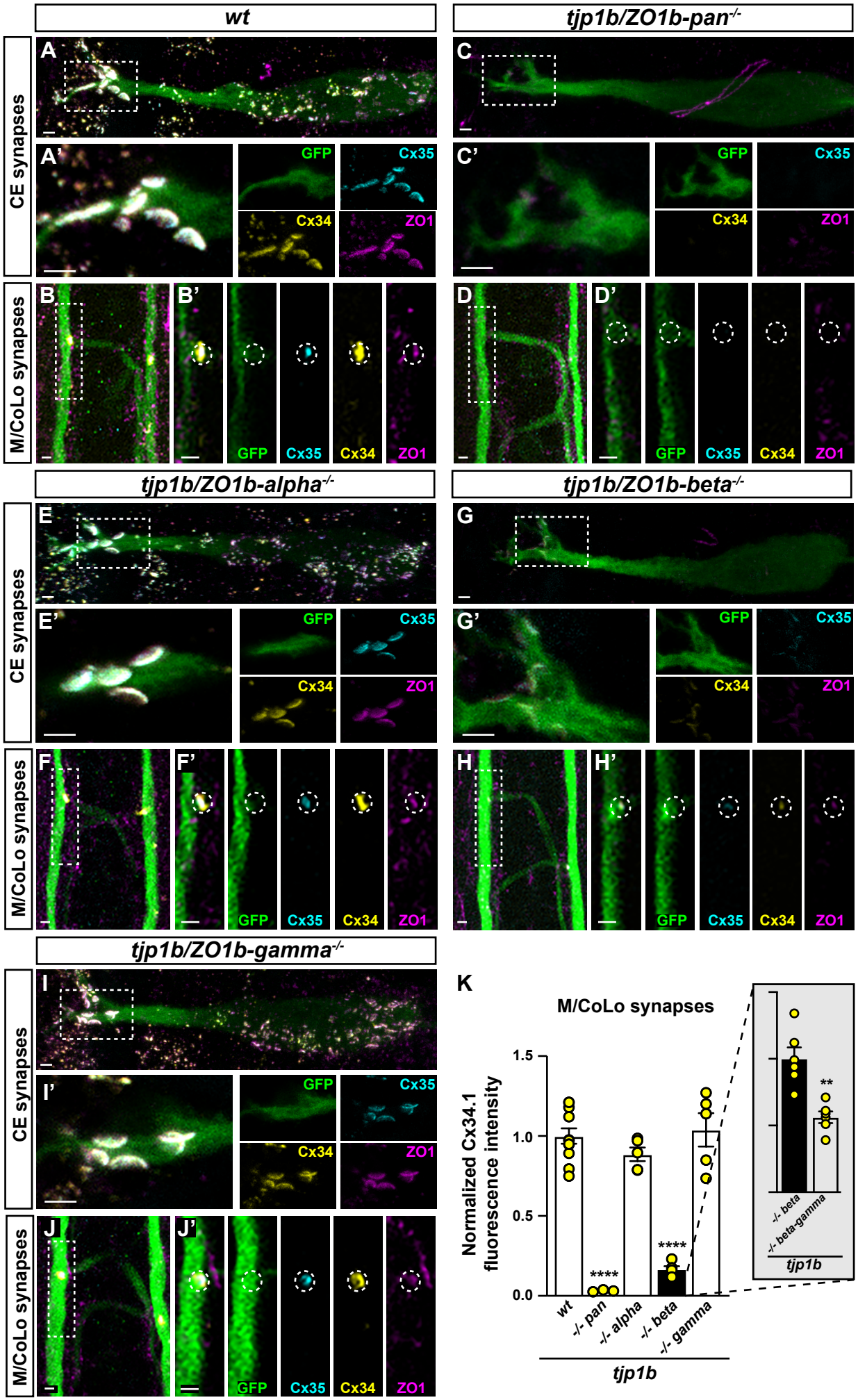
wt
tjp1b/ZO1b-pan-/-
tjp1b/ZO1b-alpha-/-
tjp1b/ZO1b-beta-/-
tjp1b/ZO1b-gamma-/-
CE synapses
M/CoLo synapses
A
A'
B
B'
C
C'
D
D'
E
E'
F
F'
G
G'
H
H'
I
I'
J
J'
GFP
Cx35
Cx34
ZO1
K
M/CoLo synapses
Normalized Cx34.1 fluorescence intensity
1.5
1.0
0.5
0.0
****
****
**
wt
-/- pan
-/- alpha
-/- beta
-/- gamma
-/- beta
-/- beta-gamma
tjp1b

Fig. S2

A

```
ZO1b Alpha  MLLSVFGGPVEEVLAGLLKLKMFGSGSKKWFIKKNKRQRTKVQRKPASGRR  51
ZO1b Beta   --------------------------------------------------  -
ZO1b Gamma  --------------------------------------------------  -

ZO1b Alpha  NKRVSRVLKRHKEVIVKQLDVSKVLPTLVYERVFTLGEYKEILGQDSSGKR  102
ZO1b Beta   --------------------------------------------------  -
ZO1b Gamma  --------------------------------------------------  -

ZO1b Alpha  AELFLDLLSQKEPAAFSAFCGVLEEVCPHLLTCFLLDGTDGSAGENKKQGQ  153
ZO1b Beta   --------------------------------------------------  -
ZO1b Gamma  --------------------------------------------------  -

ZO1b Alpha  -TKPAHSQQNALSKGQDTVCFPPMYTDPLFDTRVFPKHDKDKYGPAVYYPK  203
ZO1b Beta   MVNYQKYITVMQLALGVTAYNRDRSLPPRKHMWVFPKHDKDKYGPAVYYPK  51
ZO1b Gamma  --------------------------------------------------  -

ZO1b Alpha  FNAYIPNPDKVSVLDESEGSGHGKPSLRRIKGRIHRSKSLDSIDLLDSN   252
ZO1b Beta   FNAYIPNPDKVSVLDESEGSGHGKPSLRRIKGRIHRSKSLDSIDLLDSN   100
ZO1b Gamma  ----------------------------------------MSARAASNK     9
```

B

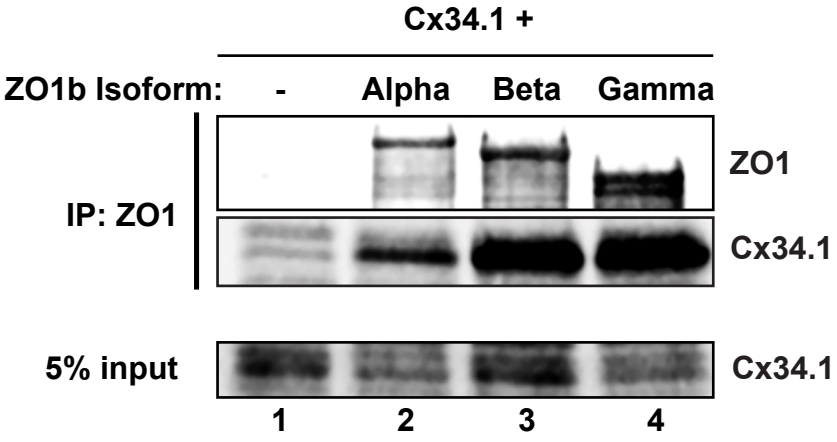

C

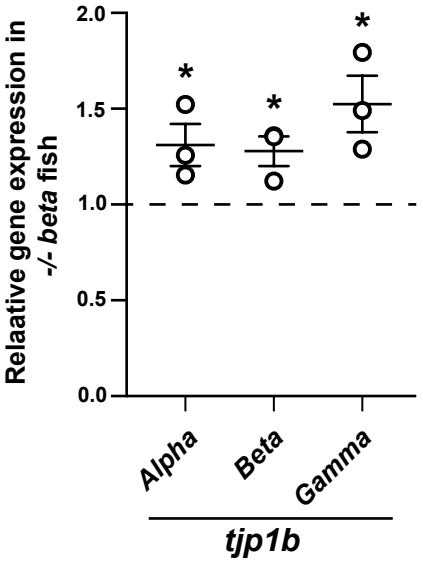

Fig. 3

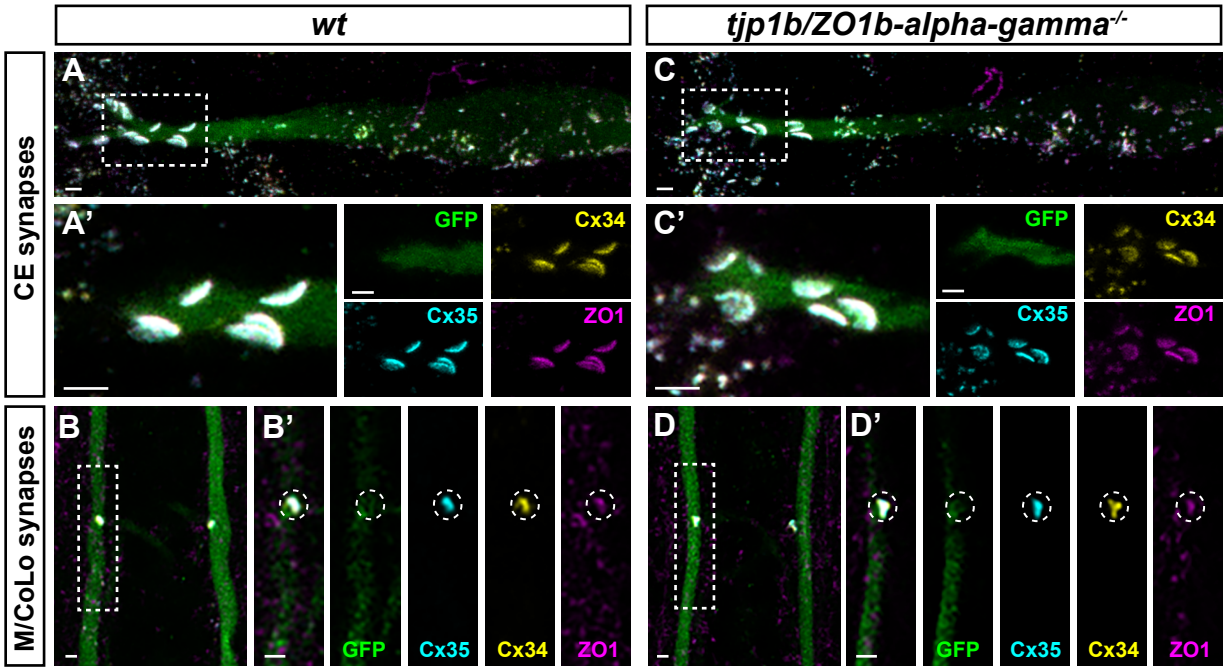
wt
tjp1b/ZO1b-alpha-gamma-/-
CE synapses
M/CoLo synapses
A
A'
B
B'
C
C'
D
D'
GFP
Cx34
Cx35
ZO1